

# Title: A Dynamic Risk Prediction Model for Rainfall-Triggered Landslides in Buncombe County, North Carolina

## **Abstract:**

Rainfall-triggered landslides are commonly occurring across the Southern Appalachians, yet effective, localized “nowcasts” that fuse dynamic precipitation with terrain characteristics remain limited. We develop a near-real-time landslide risk model for Buncombe County, North Carolina, integrating daily PRISM precipitation windows with static hydrological data. The novel dataset containing 302 mapped landslides (1981–2024) was compiled by integrating USGS DEM data and SSURGO soil information. Across models, slope was the dominant feature, while short-duration rainfall (1–7 days and 3-day maxima) most strongly increased landslide probability. In particular, 30-day cumulative rainfall often exhibited a negative association with predicted risk, suggesting that prolonged rainfall without intense surges may reduce immediate triggering. The resulting model enables county-scale, data-driven susceptibility updates based on forecasted precipitation data, offering a practical foundation for near-nowcasting and a landslide alarm system during and after intense storms.

Keywords: Rainfall-triggered landslides, Nowcasts, Buncombe County, Random Forest, XGBoost, PRISM precipitation, Landslide susceptibility modeling

[\[Link to the dataset\]](#)

## **1. Introduction**

Landslides are devastating natural hazards that take place worldwide and cause wide-ranging damage to modern society, such as human casualties, economic losses, and infrastructure damage (Froude & Petley, 2018; Kirschbaum & Stanley, 2018; Petley, 2012). In the year 2024 alone, 766 instances of landslides took place around the world, killing 4,933 individuals (Petley, 2025). Landslides across the world incur an economic cost of US\$20 billion annually, taking 17% of the yearly mean expenses caused by all natural disasters worldwide between 1980 and 2013 (Klose et al. 2016). Social infrastructures, especially transportation and communication, are highly susceptible to landslides (Sim, Lee, Remenye-Prescott, & Wong, 2022). Rural areas are likely to experience more impairments due to landslides, where these infrastructures are scarcer and scattered (Klose et al. 2015).

In search of effective landslide prediction methods, researchers have proposed various theories on the sources of these disasters, ranging from geological activity such as volcanic eruptions and earthquakes to human-induced sources such as modification of slopes and obstruction of hydrological flows (Sidle & Ochiai, 2006; Jaboyedoff et al., 2016). Among those factors, precipitation is regarded as the leading cause of landslides worldwide; extreme

rainfall triggered 70% of all landslide events across the world between 2004 and 2010 (Petley, 2012). Fittingly, the role of precipitation in landslides will only continue to grow with climate change; Gariano and Guzzetti (2016) predict that landslides triggered by rainfall will be increasingly catastrophic and recurrent as climate change increases the frequency of short, intense storm episodes. The predicted increase in landslide prevalence forebodes the urgency of an effective rainfall-induced landslide prediction model.

The Western North Carolina region has historically been dominated by rainfall-induced shallow landslides due to geographical and meteorological factors (Wooten et al., 2008). The Blue Ridge Mountains, as a part of the Southern Appalachian mountain range, are characterized by steep slope gradients (Khashchevskaya et al., 2025). Its bedrock layer mostly comprises metamorphic and igneous rocks, which, when decomposed, create saprolite, which constitutes the top layer of the horizons (Hatcher, 2010; Watterson & Jones, 2006). The saprolite-heavy soil absorbs water easily, which increases pore pressure, resulting in a higher probability of shallow landslides (Aydin, 2006). The region's geomorphic susceptibility has been called for focus again after Hurricane Helene's extensive landslide damage in Western North Carolina in 2024 (Lin et al., 2024). Allstadt et al. (2025) state that the hurricane caused unprecedented geographic disruptions in the region, particularly in Buncombe, Henderson, Rutherford, and Yancey counties. Freshwater flooding contributed to 95 of the 176 direct deaths that Helene caused, most of which were landslide-related; around 2,000 independent cases of landslides were reported to be related to Helene, with the majority located over western North Carolina (National Hurricane Center, 2025). Helene significantly damaged the communications infrastructure in western North Carolina, considering WNC's rural characteristic, which exacerbated the situation (Office of State Budget and Management, 2024). Helene's unexpected landslide damage calls for a real-time probabilistic forecasting model, localized for Western North Carolina.

At present, there is no near-nowcast model for Western North Carolina that captures dynamic changes in precipitation. In fact, nearly all of the current landslide hazard maps use minimal or no precipitation inputs. Specifically, the USGS Landslide Hazard Mapping Program's landslide susceptibility map identifies areas with elevated risk for landslips under extreme rainfall conditions (Fuemmeler et al., 2008); these, however, do not take account of real-time changes in precipitation since they were based on past correlations of landslides with geographical elements (Bauer et al., 2012). Academically, even though there have been numerous attempts at developing a physical/statistical model for the prediction of landslides (e.g., an ML-based model by Lin et al. (2024) that combines a variety of predictors such as the NC landslide database, soil surveys, digital elevation models, and water body locations), very few, if any, utilized dynamic rainfall as their primary predictor. To this end, an effective localized model of Western North Carolina for rainfall-induced landslides has proven necessary, as seen in the extensive damage Helene caused in the region.

Thus, to address the absence of a localized prediction model that incorporates dynamic rainfall variability, the proposed research will address the question: "How does incorporating static geographic data (elevation and soil depth) with the variability of rainfall data affect the

predictability of shallow landslides in the Western North Carolina region?" Ultimately, this study hopes to create an efficient prediction model in near real-time for the area, developing an early warning system for residents of Western North Carolina, specifically, Buncombe County.

Global models based on rainfall-triggered landslides have been developed and utilized for several years, with generally positive results. They are considered 'nowcasts,' because they incorporate both static geological characteristics and dynamic observations of rainfall to provide nearly real-time forecasts (Kirschbaum et al., 2012). For example, NASA's LHASA v2 model is the first operational global system to utilize dynamic satellite rainfall data along with static geological and environmental characteristics (Stanley et al., 2021). It is based on a Logistic Regression algorithm and examines static predictor variables as well as IMERG precipitation (1 km resolution) to generate probabilistic hazard labels. The new model is purported to be two-fold more accurate than the previous LHASA v1 system, which utilized a standard threshold algorithm (Kirschbaum & Stanley, 2018; NASA Earth Observatory, 2021).

Only recently the number of statistical models predicting landslides increased, from 31 in 2016 to 219 in 2024 (Ye et al., 2025). Supervised machine learning (ML) was a popular choice for its ability to capture nonlinear relationships between predictor types and landslide probability, resulting in a higher level of accuracy than conventional linear statistical models (Regorda et al., 2020). Mondini et al. (2023) developed a time-dependent landslide model based on Italy. Exploiting RNN's strength in sequential data, they used continuous rainfall data for a window of 30 days, excluding geological or environmental factors. Similarly, Chan et al. (2018) built a logistic regression-based model aimed at predicting landslides caused by a typhoon's heavy rain in the southern region of Taiwan. The model mainly used runoff flow depth, not pure precipitation data, taking into account soil saturation, which reached an accuracy of 80~85%. Kang et al. (2024) recently constructed a localized model for Yunnan Province, China, with its Random Forest model reaching an accuracy level of 0.906. Incorporating every aspect of geographic, environmental and hydrological factors into eight variables. All the above ML-based models center around rainfall data. Their high accuracy levels affirm the need for dynamic rainfall data in a localized landslide model.

Focusing on North America, Thomas et al. (2019) challenged if satellite rainfall data can replace in situ hydrological data to evaluate the soil saturation threshold for a slope failure, reflecting a recent trend of increasing remote geospatial data-based models (Akosah et al., 2024). The findings from this localized model of California demonstrated that rainfall (specifically satellite-measured rainfall data) cannot be relied upon to predict landslides and encourage a hydrogeological gauge that calibrates rainfall data with on-site hydrologic data to develop a soil wetness index. Other studies that support the aforementioned findings include a comprehensive model (Lee et al., 2023) blending precipitation duration/intensity and normalized soil moisture capacity, which dropped false alarms (FA) from ~26 to 3. Both studies emphasize the importance of contextualizing raw rainfall data with local hydrologic features in evaluating the soil saturation level.

The contribution of this study is twofold. We build a localized, near-real-time landslide prediction model. For the modeling, an equal number of non-events were randomly chosen based on the landslide inventory of Buncombe County (North Carolina Department of Environmental Quality, 2024). To avoid pattern biasing in specific constellations of events, stratification and a spatial block cross-validation approach were utilized. Three different ML algorithms were tested overall, with three models per algorithm (F0, F1, and F2) based on feature type. The assessment of performance and feature analysis was interpreted using evaluation metrics, SHAP plots, and permutation importance.

To fit and evaluate the model, we designed a hydrologic/environmental dataset that collates daily precipitation data (PRISM Climate Group, 2024), a topography map (USGS DEM), and soil depth (USDA SSURGO). The dataset is open and available for further research at the specified repository.

The next section describes the datasets and methodology of the research. Section 3 illustrates the results of the findings. Section 4 delivers the conclusion of the research.

## **2. Data and Methodology**

### **Dataset**

This research aimed to create a dynamic prediction model localized in Buncombe County, North Carolina, geographically located within the Blue Ridge Mountains (Figure 2a). The inventory of landslide events was extracted from the North Carolina Landslide Points dataset (via NC OneMap; North Carolina Department of Environmental Quality, 2024). The dataset included event geometry (points) and traceability fields: *IsLandslide* (event flag), *Event\_Date*, *Sort\_Date*, *X*, *Y*, *County*, *GlobalID*, *OBJECTID*, *Data\_Type*, and *Source\_Period*. The inventory was both a temporal anchor (*Event\_Date*) for rainfall-window calculations referred to by dates and a spatial anchor (*X*, *Y*) for topography and soil data extraction. Additionally, an equal number of non-event samples were created for control, randomly selecting the same time (January 1981–December 2021) and same region of interest (Buncombe County) as those in the landslide dataset. Ultimately, equal numbers of events and non-events were included in the final dataset used for modeling.

Gridded precipitation (4 km resolution) was extracted from PRISM daily products (PRISM Climate Group, 2024) throughout the entire analysis period (spanning from January 1981 to December 2024). Using the reference dates of the events and non-events—the event date (*Event\_Date*) or the control (*Random\_Date*)—historical sums over windows of 1-day (*R1d*), 3-days (*R3d*), 7-days (*R7d*), and 30-days (*R30d*) were computed. Other temporal windows included maximum rainfall sums calculated for both 3-day (*Max\_Rainfall\_3day*) and 30-day (*Max\_Rainfall\_30day*) intervals. All precipitation measurements were in units of millimeters,

and all the calculation windows' end dates coincided with the reference date of the observation (Table 1 contains the definition and sources of all features).

Topography was taken from a DEM (Digital Elevation Model) encompassing Buncombe County published by the U.S. Geological Survey (2022). The DEM already provided elevation (*Elevation\_m*), while slope (*Slope\_deg*) was computed from Horn's (1981) 3×3 finite difference gradients and converted into degrees (Figure 2; Equations 1, 2, and 3).

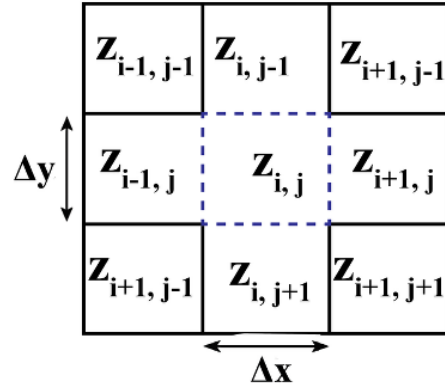


**Figure 1.** Visualization of Horn's (1981) 3×3 finite difference gradient calculator.  $Z_{i,j}$  symbolizes the position of the elevation of a particular cell.  $\Delta x$  and  $\Delta y$  are the horizontal and vertical grid distances of the cells.

$$p = [(z_{i+1,j-1} + 2z_{i+1,j+1} - z_{i-1,j-1}) - (z_{i+1,j+1} + 2z_{i-1,j} + z_{i-1,j+1})] / 8\Delta x \quad (1)$$

$$q = [(z_{i-1,j+1} + 2z_{i,j+1} - z_{i+1,j+1}) - (z_{i-1,j-1} + 2z_{i-1,j} + z_{i-1,j-1})] / 8\Delta y \quad (2)$$

$$Slope = \tan^{-1}(\sqrt{p^2 + q^2}) \quad (3)$$

The values  $p$  and  $q$  in Equations 1 to 3 represent the rate of elevation change in the east-west direction and the north-south direction, respectively. The DEM cell resolution for Buncombe County showed an equal width and height of 40 meters. To avoid unit discrepancy across different datasets, all datasets were under a consistent projected coordinate reference system (NAD83/North Carolina; EPSG:32119) and maintained a resolution of 40m.

Soil data originated from USDA NRCS SSURGO map units (U.S. Department of Agriculture, Natural Resources Conservation Service, 2024). A point-polygon comparison was used to match MUKEY and MUSYM to each sample point, linking depth information from the related tables. Soil depth was converted to a numeric variable (*Soil\_Depth\_cm*) by extracting data from raw strings (*Soil\_Depth\_cm\_raw*) and converting the variable into a binary flag

(*Soil\_Depth\_Deep200\_Flag*), where entries larger than 200 were changed to 1, while any other entries were changed to 0. These soil properties were viewed as static covariates that reflect conditions of regolith associated with instability triggered by rainfall.

For map compilation and masking, administrative boundaries by county were employed to clip rasters and to define the sampling window for controls with a modest buffer to attenuate edge effects (U.S. Census Bureau, 2022). Land cover from NLCD was retained for descriptive mapping and voluntary sensitivity tests but was not included in the baseline prediction set (U.S. Geological Survey, 2021).

Gridded variables such as rainfall windows, elevation, and slope were sampled by bilinear interpolation at coordinates defined by points (X, Y) (Burrough & McDonnell, 1998). Soil data, specifically soil depth, came from the MUKEY and MUSYM area codes. Units of measurement have been standardized with precipitation in millimeters, elevation in meters, and slope measured in degrees. We verified the rainfall windows to check that the end dates coincide with the event reference date. Data instances with missing values were removed from the dataset.

The dataset created is a linked dataset, combining information from PRISM daily rainfall data, the USGS DEM, and the USDA SSURGO map specific to Buncombe county, and can be used for further analyses related to landslide risk. Linking information from the various datasets was not trivial, as it required gathering chronological information and summarizing it for the selected data points before linking it to the main dataset (Longley et al., 2015; Burrough & McDonnell, 1998). Other challenges included incompatible reference systems that had to be reconciled. The complete dataset includes the outcome variable (*IsLandslide*) and full fields for past rainfall, topography, and soil depth with comprehensive metadata for provenance and audit purposes, which comprises *Event\_Date/Random\_Date*, *X*, *Y*, *County*, *GlobalID*, *OBJECTID*, *Data\_Type*, *Source\_Period*, *MUKEY*, *MUSYM*, and *Soil\_Depth\_cm\_raw*.

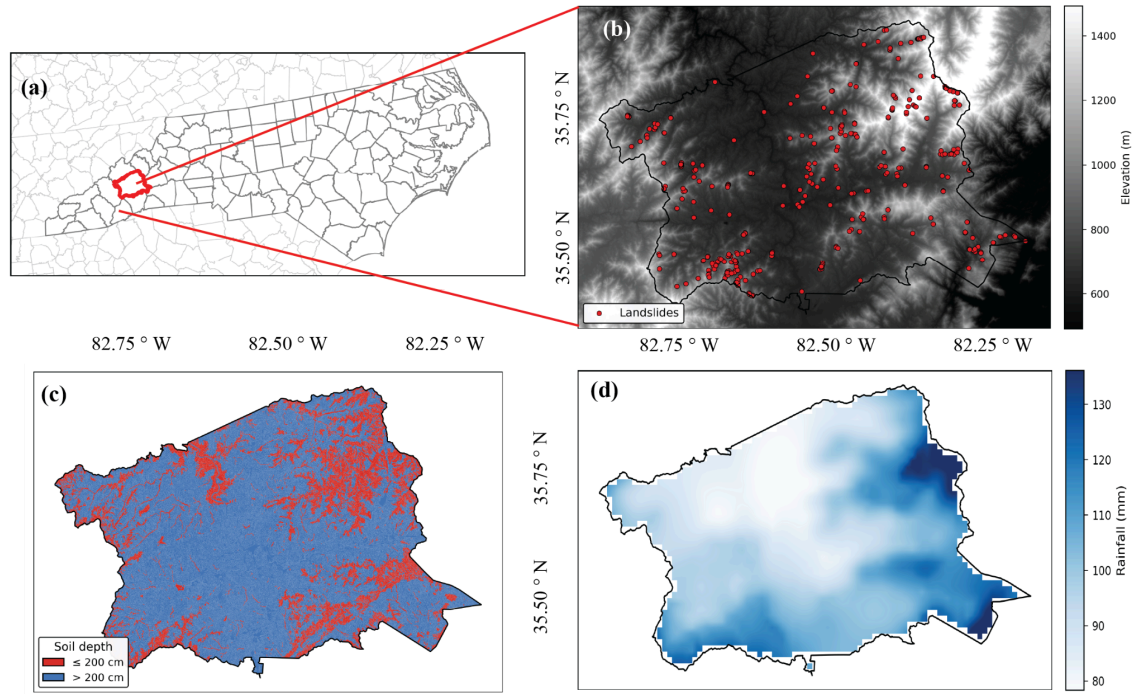


**Figure 2:** (a) Geographical location of the study area, (b) elevation, (c) soil depth, (d) 30 year average rainfall.

Symbol (unit)	How it was calculated	Source
<i>R1d</i> (mm)	Sum of daily PRISM rainfall for 1 day	PRISM (800m)
<i>R3d</i> (mm)	Sum of daily PRISM rainfall for 3 days	PRISM (800m)
<i>R7d</i> (mm)	Sum of daily PRISM rainfall for 7 days	PRISM (800m)
<i>R30d</i> (mm)	Sum of daily PRISM rainfall for 30 days	PRISM (800m)
<i>Max_Rainfall_3day</i> (mm)	Rolling maximum of 3-day totals in past 30 days	PRISM (800m)
<i>Max_Rainfall_30day</i> (mm)	Rolling maximum of 30-day totals in past 90 days	PRISM (800m)
<i>Elevation_m</i> (m)	Extracted directly from DEM	USGS DEM (40m)
<i>Slope_deg</i> (°)	Derived from DEM using slope algorithm	USGS DEM (40m)
<i>Soil_Depth_Deep200_Flag</i> (—)	Flag for soils deeper than 200 cm	SSURGO Soil

**Table 1:** Features definitions (Rainfall time-frames are from the reference point of the corresponding event)

All data collection, processing and model development steps were done in Python 3.9 in the PyCharm IDE. Libraries, including NumPy, Pandas, SciPy, Matplotlib, and Seaborn, were used for scientific computing; GeoPandas, Shapely, and Rasterio were used for data processing; and scikit-learn and XGBoost models combined with SHAP were chosen for model development and assessment. The models were run on a Mac Apple M2 processor.

## Modeling

To assess which rainfall variables specifically influenced landslide probability, the temporal accumulation/maximum rainfall predictors were analyzed with all non-empty possible combinations. A primary concern was minimizing overfitting due to the large number of rainfall predictors (*R1d*, *R3d*, *R7d*, *R30d*, *Max\_Rainfall\_3day*, *Max\_Rainfall\_30day*). Thus, a training–test split was implemented via a stratified five-fold cross-validation approach using a constant seed and data point shuffling. In addition, the evaluation was repeated for every rainfall predictor subset. The model that showed the most accurate predictions on the test data was included in the final comparison across other types of models. The above processes were independently conducted for each machine learning (ML) algorithm model.

Three separate ML algorithms were employed for the actual study—Logistic Regression, Random Forest and XGBoost (Breiman, 2001; Chen & Guestrin, 2016). Due to logistic regression's simple and linear design, the model was effective in serving as a benchmark to compare with nonlinear models. The performance of the model was quantified through ROC curves, confusion tables, and summary measures: accuracy, precision, recall, ROC–AUC, and the Brier score (Brier, 1950). For logistic regression, the coefficient magnitudes summarized how each variable influenced the model prediction, while standard errors, p-values and confidence intervals measured the degree of statistical significance of that prediction.

A Random Forest algorithm was used as the baseline nonlinear model. Interpretation of the model involved a combination of intrinsic feature importance as well as SHAP analysis. Intrinsic feature importance was determined as the mean decrease in impurity, indicating the effectiveness of each predictor in splitting the data. Shapley values for each variable and data point were illustrated via SHAP bar plots, SHAP beeswarm plots and SHAP waterfall plots per sample (Lundberg & Lee, 2017). The bar plot visualized the average contribution of each feature to the overall prediction, while the beeswarm plots showed both the distribution as well as the direction of the predictor contributions. SHAP waterfall plots gave local explanations regarding the most likely landslide samples. A full dataset, including SHAP values as well as both the imputed and the original feature values, expected values, probabilities, and true labels, in addition to original metadata, was also provided so that both global and case-specific insights could be obtained. Model discrimination as well as calibration were also assessed as part of ROC curves and confusion matrices, as well as the same summary metrics that were used as part of Logistic Regression.

In answering the hypothesis, three separate models were created for each type of ML algorithm. Model F0 used just slope and elevation, aiming to assess the predictive potential



based on the static predictor: terrain alone. Model F1 added rainfall accumulation intervals, alongside slope and elevation, as the basis to also evaluate the short- as well as longer-term rainfall triggers. Following on from F1, Model F2 also included soil depth so that the effect of the subsurface interacting with both rainfall and the terrain factors could be determined. Each algorithm was then trained across the three feature settings, ultimately leaving us with parallel models that allowed a direct comparison.

The F0, F1, and F2 configurations for each model (Logistic Regression, Random Forest, and XGBoost) were trained and tested on the same sample and therefore any discrepancies in results were not driven by sampling but rather variable differences.

Comparison analysis conducted on XGBoost involved classification accuracy, showing ROC curves and confusion matrices, as well as the complete set of metrics, including accuracy, precision, recall, F1 score, and ROC-AUC, as well as the Brier score. Interpretable techniques, such as SHAP dependence plots or permutation importance, are only presented for the Random Forest model.

### **3. Results and Discussion**

The compiled landslide dataset contained 9,092 events recorded within North Carolina between 1940 and 2024, of which 398 occurred within the study area of Buncombe County (Figure 3). Because the PRISM Weather daily rainfall data before 1981 was unavailable for the public, the inventory was limited to the time frame between 1981 and 2024, limiting the data points to 302 landslide events. Corresponding to these landslide points, an equal number of control points were created by sampling sites and dates randomly within the same county and time frame. As such, the final dataset contained 604 total entries, split evenly between events and controls, thus reducing potential biases for certain variables and increasing its robustness toward new data.

All the records had a collection of hydrological covariates. Rainy features comprised both cumulative windows (*R1d*, *R3d*, *R7d*, *R30d*) as well as highest intensities (*Max\_Rainfall\_3day*, *Max\_Rainfall\_30day*). Geological features included elevation as well as slope at 40 m resolution. Soil depth was included as an added predictor expressed as a binary flag (>200 cm vs. ≤200 cm), as the vast majority of the sites had extremely deep soils.

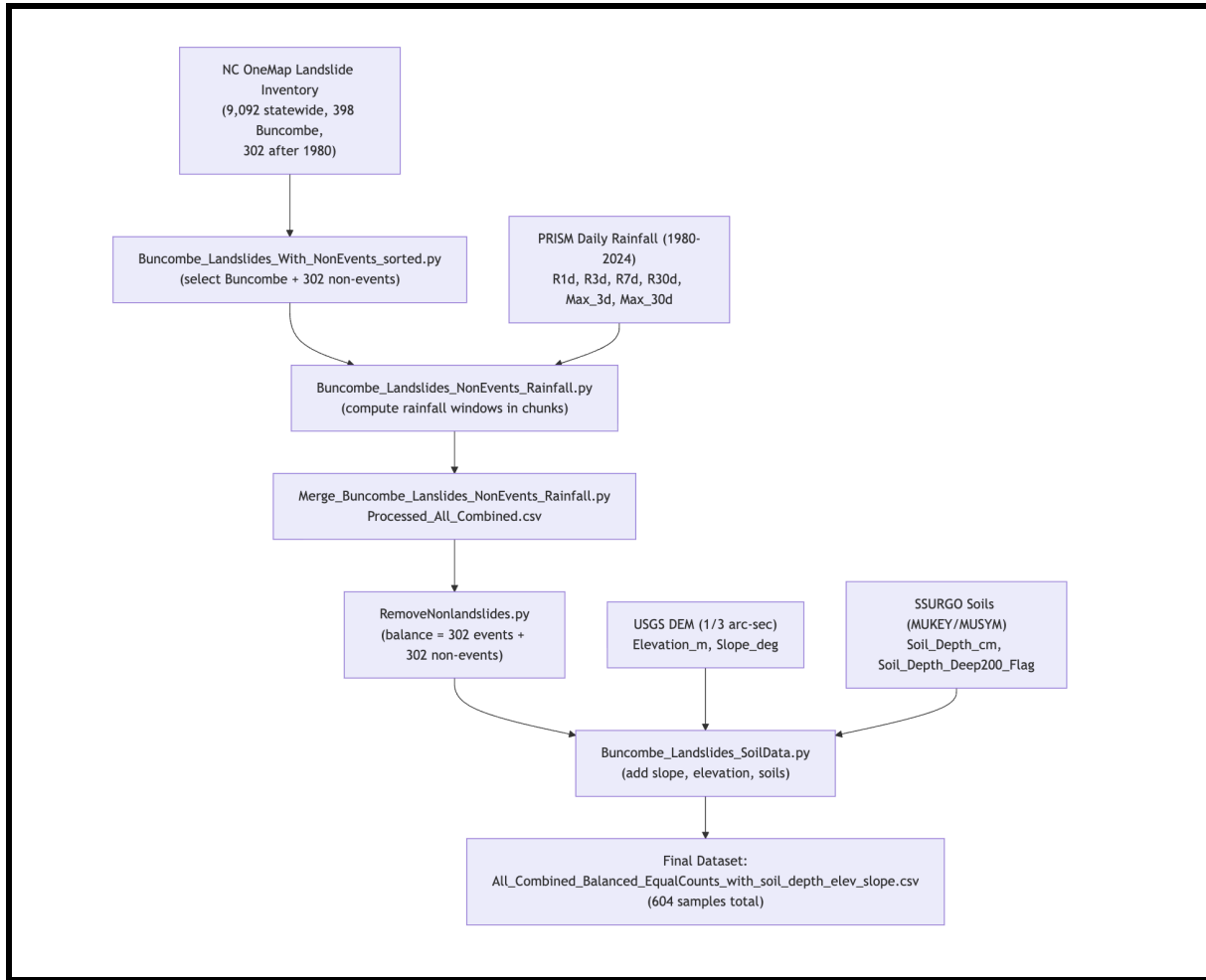


**Figure 3:** Flowchart of landslide events and non-events data processing

The final dataset merged the rainfall, terrain, and soil characteristics for each observation. Its well-balanced design (302 events + 302 controls) ensured the risk of class bias was kept small, and the range of covariate variability enabled the models to incorporate long-term conditioning factors (e.g., slope, soil depth) as well as short-term triggers (e.g., extreme rains).

### Feature selection:

Feature selection indicated consistency across the nonlinear and the linear models. In the Logistic Regression category, the optimum subset of rainfall data comprised *Max\_Rainfall\_30day*, *R3d*, *R7d*, and *R30d*, achieving an accuracy of 0.593 as well as an ROC-AUC of 0.614 (see Table 2). Short-period rainfall accumulation, including three-day as well as seven-day buildup, was frequently shown in the top-ranking combinations, showing how these predictors have a strong relationship with landslide risks. However, long-term predictors such as *Max\_Rainfall\_30day* and *R30d* also showed up occasionally, albeit not as frequently as short-term variables.

Logistic Regression (Top 5)	Accuracy	ROC-AUC
<i>Max_Rainfall_30day, R3d, R7d, R30d</i>	0.593	0.614
<i>Max_Rainfall_30day, Max_Rainfall_3day, R3d, R7d</i>	0.589	0.621
<i>Max_Rainfall_30day, R1d, R3d, R7d, R30d</i>	0.589	0.613
<i>Max_Rainfall_30day, R7d, R30d</i>	0.584	0.600
<i>Max_Rainfall_30day, Max_Rainfall_3day, R1d, R7d, R30d</i>	0.584	0.619

**Table 2:** Top-performing subsets of Rainfall Features for Logistic Regression

Random Forest (Top 5)	Accuracy	ROC-AUC
<i>Max_Rainfall_30day, Max_Rainfall_3day, R1d, R3d</i>	0.808	0.888
<i>Max_Rainfall_30day, R1d, R7d, R30d</i>	0.806	0.882
<i>Max_Rainfall_30day, R3d, R7d, R30d</i>	0.805	0.890
<i>Max_Rainfall_30day, Max_Rainfall_3day, R1d, R3d, R7d</i>	0.801	0.890
<i>Max_Rainfall_30day, Max_Rainfall_3day, R1d, R7d, R30d</i>	0.801	0.883

**Table 3:** Top-performing subsets of Rainfall Features for Random Forest

In the Random Forest output, the best-performing subset included *Max\_Rainfall\_30day*, *Max\_Rainfall\_3day*, *R1d*, and *R3d*, yielding exceptional accuracy up to 0.808 and ROC-AUC reaching as high as 0.888 (see Table 3). Moreover, subsets including *R3d* and *R7d* also appeared among the very best, a point also supported by the results yielded by the Logistic Regression (see Table 2). However, the Random Forest model also brought to light that short-term rainfall predictors like *R1d* as well as the *Max\_Rainfall\_3day* significantly improved classification, bringing to the forefront nonlinear interactions. These findings indicated that although both nonlinear and linear prototypes invariably recognized the paramount significance of short-term rainfall, the Random Forest technique, in addition, captured the additional nuances of the lengths of the rainfall affecting the probabilities of the landslide occurrences (refer to Table 3).

### Actual Models:

Logistic Regression:

FeatureSet	Accuracy	Precision	Recall	F1 Score	ROC_AUC	Brier
F0	0.620	0.609	0.650	0.629	0.673	0.229
F1	0.702	0.688	0.733	0.710	0.771	0.193
F2	0.702	0.682	0.750	0.714	0.775	0.191

**Table 4:** Logistic Regression model performance across feature sets (F0, F1, F2).

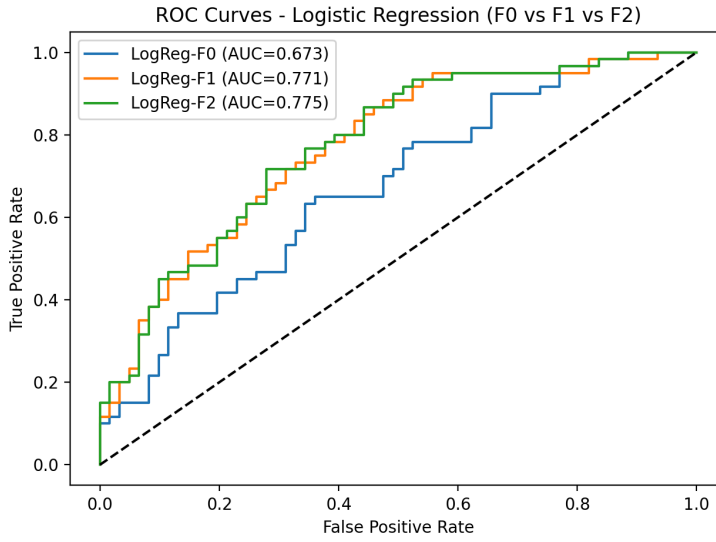


**Figure 4:** ROC Curves for the three models F0, F1, and F2 Logistic Regression.

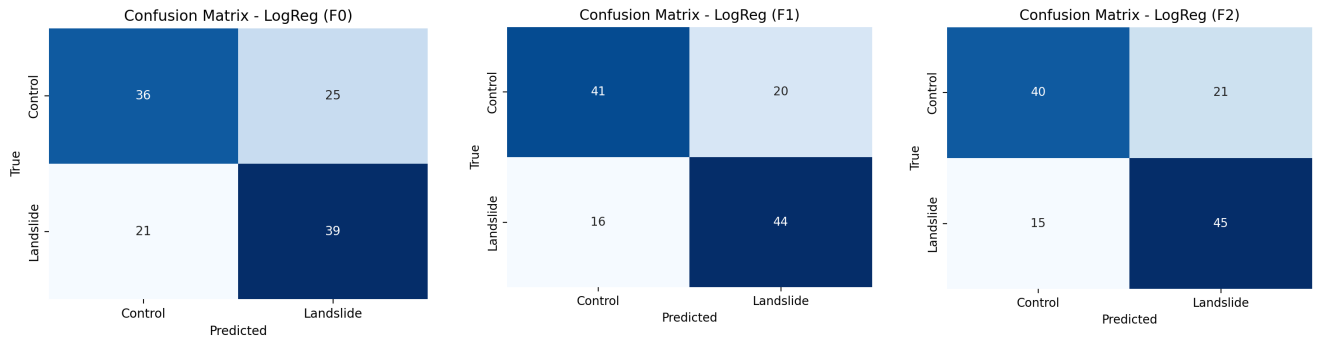


**Figure 5-7:** Confusion Matrices of F0, F1, F2 Logistic Regression Models

Feature	F0	F1	F2
<i>Slope_deg</i>	0.7150	1.3574	1.3813
<i>Max_Rainfall_30day</i>	-0.7287	0.5666	0.5871
<i>R30d</i>	0.2208	-0.5968	-0.6327
<i>R7d</i>	-0.1018	0.2192	0.2136
<i>Elevation_m</i>		-0.1886	-0.1099
<i>R3d</i>		-0.0571	-0.0620
<i>Soil_Depth_Deep200_Flag</i>			0.1943

**Table 5:** Regression coefficients for each feature of F0, F1, F2 Logistic Regression Models

Performance for Logistic Regression got progressively better as more predictors were added (Table 4). In the terrain-only version F0, accuracy was 0.62 with an AUC of 0.67. Inclusion of the rainfall predictors in F1 got the accuracy up to 0.70 and the AUC up to 0.77. Inclusion of the full set of predictors in the complete version F2 got the best accuracy at 0.70 as well as the best AUC at 0.78. All of these trends carry through on the ROC curves (Figure 4) as well as the confusion matrices (Figures 5-7): F0 got 36 controls and 39 landslide cases correct, but F2 got 40 correct controls as well as 45 correct landslides.

Model interpretation relied on the regression coefficients (Table 5). The slope was the strongest predictor variable, followed closely by *Max\_Rainfall\_30day*, both having a positive effect on the risk of landslides, except for the F0 model. Here, the cumulative 30-day rainfall (*R30d*) tended to have a negative coefficient, meaning long-term accumulation did not significantly increase the probability of slope failure after accounting for short-term accumulation or extreme events. These results strengthen the conclusion that the best explanation for landslides lies in the interaction between the region's steep slope and short-term, high-rate bursts of rain, shown in the Brier Scores of Table 4.

Random Forest:

FeatureSet	Accuracy	Precision	Recall	F1 Score	ROC_AUC	Brier
F0	0.661	0.679	0.623	0.650	0.741	0.216
F1	0.810	0.797	0.836	0.816	0.888	0.139
F2	0.785	0.778	0.803	0.790	0.880	0.144

**Table 5:** Random Forest model performance across feature sets (F0, F1, F2).

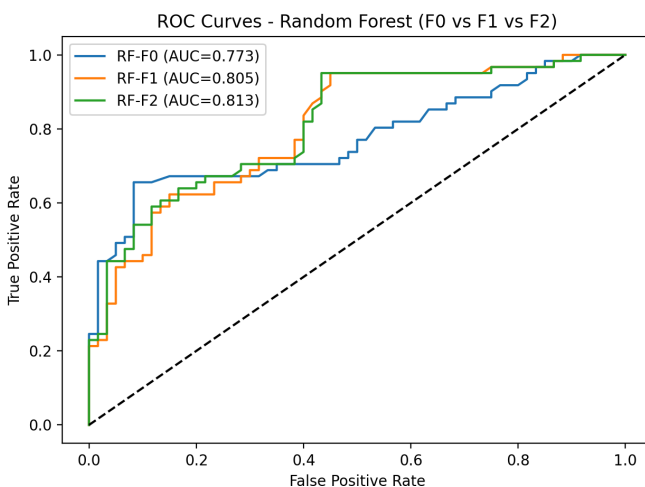


**Figure 8:** ROC Curves for the three models F0, F1, and F2 of Random Forest.

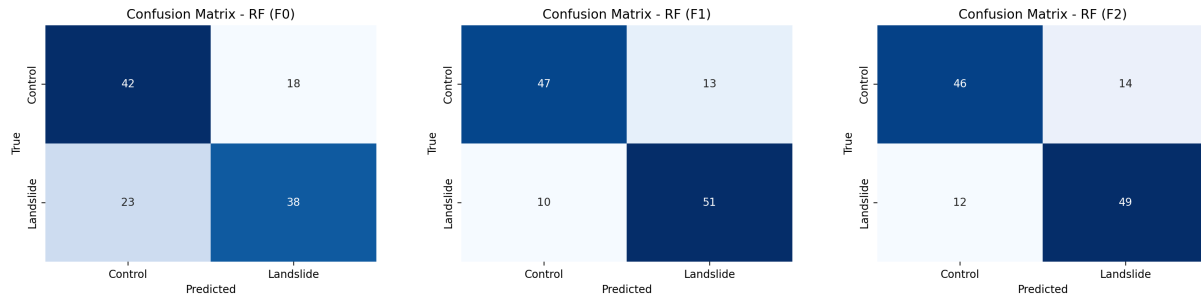


**Figure 9-11:** Confusion matrix of the three models F0, F1, and F2 of Random Forest.

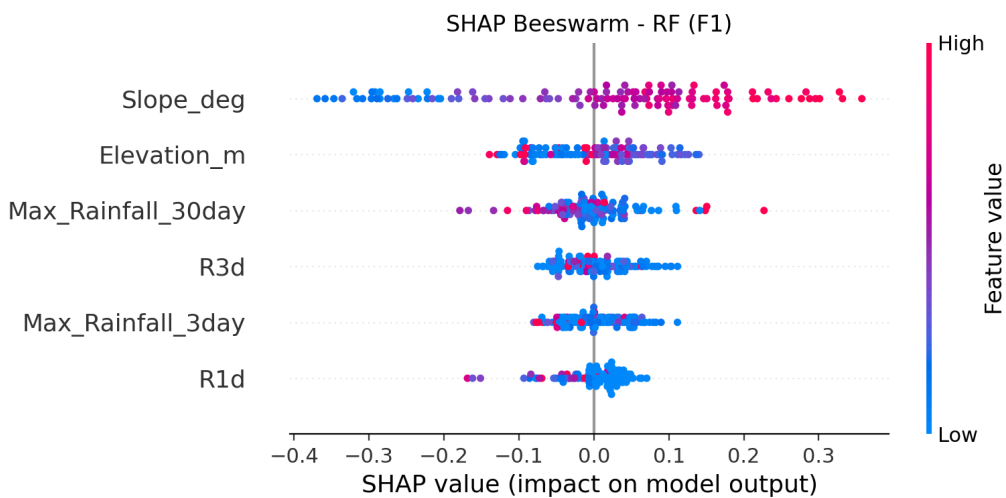


**Figure 12:** SHAP Beeswarm Chart for the F1 Random Forest Model.

The best-performing model, out of all three algorithms, was the Random Forest (RF) model. They were consistent across varying combinations of features (Table 5; Figure 8). Although the accuracy of the F0 model was 0.66 and the AUC 0.74—still notably higher than the accuracy of the Logistic Regression (LR) model—the F1 model setup, incorporating rainfall data, gave an accuracy of 0.81 and an AUC of 0.89, demonstrating the best performance of all. But the introduction of the soil feature in F2 detracted from the performance to an accuracy of 0.79 and an AUC of 0.88, departing from the trends of the LR. Still, the decrease in performance still holds that soil depth holds insignificant influence in prediction, especially for RF algorithms.

Considering F1's superior performance, feature analysis was only conducted on the F1 model, focusing on SHAP figures (Figure 12). The figure confirmed that slope is the primary predictor, exerting the most influence on the model. Subsequently, it was followed by *R30d*, *elevation*, and short-term rainfall features such as *R7d*, *Max\_Rainfall\_30day*, and

*Max\_Rainfall\_3day*. According to the SHAP beeswarm plot (Figure 12), slope indicated a positive relationship with the risk of landslides, while elevation showed a bidirectional influence. Short-term bursts of rain, along with extreme maxima, exerted tremendously powerful effects in increasing the probability; conversely, cumulative rains over a 30-day period revealed a negative outcome, which diminished the likelihood of landslide occurrence.

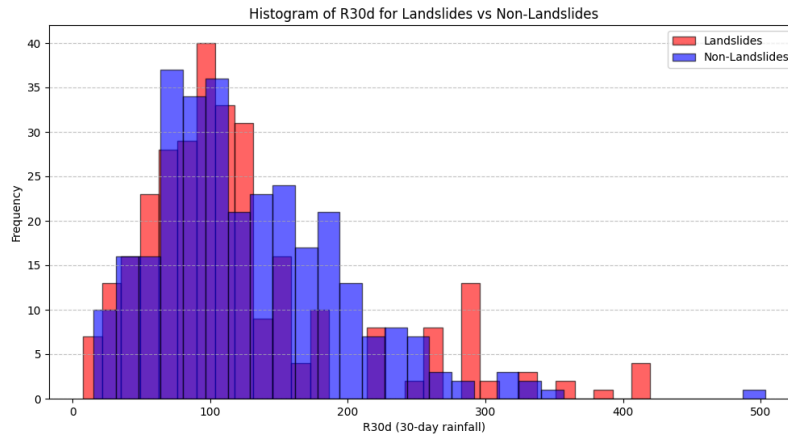


**Figure 13:** Distribution of 30-Day Cumulative Rainfall (R30d) for Landslide and Non-Landslide Events

As shown in the R30d histogram (Figure 13), both distributions of rainfall values were comparable, confirming that rainfall data were similarly distributed across both categories, thus strengthening the model's credibility. These findings underscore the capability of Random Forest to capture both anticipated and unexpected dynamics regarding landslide susceptibility. Intriguing is the discovery of the negative correlation between long-term cumulative rains and the model's predicted likelihood. This suggests that long-term rain accumulation, when not accompanied by brief extremes, may actually contribute to stabilizing the slope by facilitating gradual infiltration and percolation before pore pressurization persists long enough to initiate brief shallow failures. The results derived match past works citing landslide behavior on highly stepped landscapes as being mostly due to short-term high-magnitude events instead of being entirely the product of prolonged wet spells (e.g., Crozier, 2010; Tiranti & Rabuffetti, 2010; Bogaard & Greco, 2018). In addition, the decreased performance for F2 implies soil depth had little bearing on enhancing predictive performance at the particular resolution utilized in this study. In conclusion, the results from applying the Random Forest model indicate that the landslide hazard in Buncombe is primarily caused by a combination of a highly stepped landscape on slope discontinuities and short periods of increased rainfall, rather than long periods of rainfall acting as an instantaneous trigger.

## XGBoost

FeatureSet	Accuracy	Precision	Recall	F1 Score	ROC_AUC	Brier
F0	0.711	0.719	0.683	0.701	0.814	0.179
F1	0.802	0.757	0.883	0.815	0.879	0.141
F2	0.802	0.765	0.867	0.813	0.885	0.138

**Table 6:** XGBoost model performance across feature sets (F0, F1, F2).

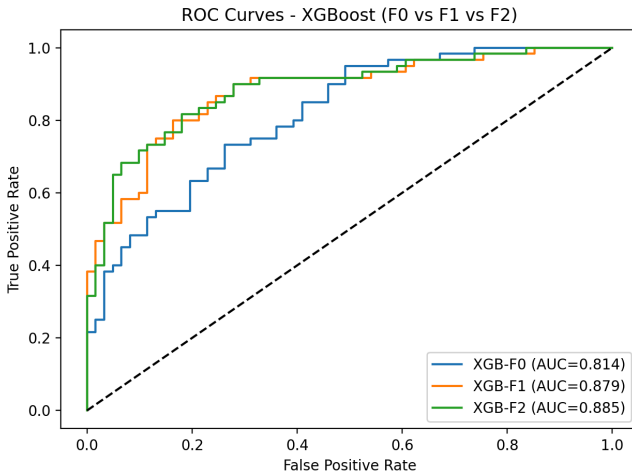


**Figure 14:** ROC curves of the three XGBoost models, F0, F1, and F2.

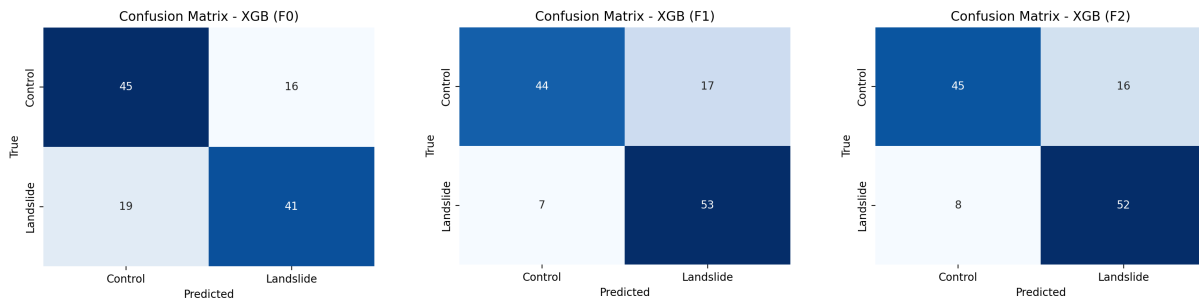


**Figure 15-17:** Confusion Matrix of the three models F0, F1, and F2 of XGBoost.

Surprisingly, XGBoost did not outperform the random forest model—instead, its F1 and F2 models showed similar prediction accuracy to the Random Forest Model (Table 6; Figure 14). The F0 XGBoost architecture excelled in model strength through an accuracy of 0.74 and an AUC of 0.81 in comparison to the other two F0 methods: Logistic Regression (LR) (accuracy 0.62, AUC 0.67) and Random Forest (RF) (accuracy 0.66, AUC 0.74). As expected, adding rainfall features improved the accuracy to 0.80 and AUC to 0.88, still better than the LR model, yet similar to the performance of the RF model (accuracy: 0.81, AUC: 0.89). Likewise, these trends appear to the full model (F2) equivalently. The full model (F2), which



incorporated soil depth, produced the highest overall performance with an accuracy of 0.82 and an AUC of 0.89. The confusion matrix for F2 (Figure 17) highlights its balance, correctly classifying 45 controls and 52 landslides.

Compared to Logistic Regression and Random Forest, XGBoost delivered higher accuracy and consistently stronger AUC across feature sets, confirming its robustness in handling complex nonlinear relationships. The results reinforce that steep slopes and short-term rainfall extremes are primary triggers, while long-term rainfall can act as a dampening factor rather than a direct trigger (Crozier, 2010; Bogaard & Greco, 2018). The improved performance of the full F2 model also suggests that soil depth, while secondary to slope, provides additional predictive power in boosted frameworks.

Accuracy improved across all models when rainfall was added to terrain predictors. Logistic Regression rose modestly from 0.62 (F0) to 0.70 (F2), Random Forest increased more sharply from 0.66 (F0) to 0.81 (F1) but dropped slightly with soil depth (0.79, F2), while XGBoost achieved the highest accuracies at every stage, from 0.74 (F0) to 0.82 (F2).

### Conclusions:

This study developed a localized near-real-time landslide prediction framework for Buncombe County, North Carolina, using machine learning models and environmental predictors. By compiling a balanced dataset of 302 landslides and 302 non-events, rainfall windows from PRISM, topography from USGS DEMs, and soil depth from SSURGO, we trained Logistic Regression, Random Forest, and XGBoost classifiers. The pipeline incorporated stratified and spatial-block cross-validation, allowing us to rigorously compare models while preserving spatial representativeness. SHAP analysis and intrinsic feature importance made it possible to understand how predictors shaped landslide susceptibility in this mountainous region.

Across models, Random Forest consistently achieved the highest predictive performance (accuracy ≈ 0.82, AUC ≈ 0.89), followed by XGBoost and Logistic Regression. In all frameworks, slope emerged as the dominant predictor, confirming prior work showing terrain steepness as the primary control on landslide occurrence (Zheng et al., 2025; Xiao et al., 2024). Short-term rainfall accumulations (1–7 days, maxima over 3 days) were strongly associated with failures, consistent with global findings that intense short-duration rainfall is the principal trigger for shallow landslides (Crosta, 2004; Pennington et al., 2014; Barthélemy et al., 2024). A notable theoretical contribution was the identification of long-term cumulative rainfall (R30d) as a *negative* predictor in several models, suggesting that extended wet periods may sometimes stabilize slopes by allowing gradual drainage and infiltration rather than immediate pore-pressure buildup (Crosta, 2004; Fan et al., 2020). Soil depth contributed marginally, adding value only in boosted frameworks, which echoes recent findings that subsurface factors are often secondary to slope–rainfall interactions (Lee et al., 2023).

These results underscore both the practical and scientific value of localized machine-learning-based landslide modeling. The framework demonstrates that integrating rainfall windows with terrain predictors can generate near-real-time susceptibility maps, offering actionable information for hazard managers after storms like Hurricane Helene. At the same time, the findings reinforce a broader theoretical consensus: steep slopes combined with short-term rainfall extremes are the key drivers of shallow failures, while long-term rainfall plays a preparatory but not directly triggering role (Pennington et al., 2014; Gariano & Guzzetti, 2016). Limitations of this study include a simplified binary soil depth representation, a relatively small sample size, and a lack of landslide-type differentiation. Future work should incorporate higher-resolution soil and land cover data, expand temporal coverage with satellite rainfall products, and test the transferability of this framework across Western North Carolina. Ultimately, coupling such models with rainfall forecasts could enable truly real-time landslide “nowcasting,” a direction increasingly emphasized in both local and global hazard research (Stanley et al., 2021; Khan et al., 2022).

#### Bibliography:

Akosah, S., Gratchev, I., Kim, D.-H., & Ohn, S.-Y. (2024). Application of Artificial Intelligence and Remote Sensing for Landslide Detection and Prediction: Systematic Review.

*Remote Sensing*, 16(16), 2947. <https://doi.org/10.3390/rs16162947>

Allstadt, K., McBride, S. K., Godt, J., Slaughter, S., Baxstrom, K., Sobieszczyk, S., & Stull, A.

(2025). *Preliminary field report of landslide hazards following Hurricane Helene*

(Report Nos. 2025–1028; Open-File Report). USGS Publications Warehouse.

<https://doi.org/10.3133/ofr20251028>

Aydin, A. (2006). Stability of saprolitic slopes: Nature and role of field scale

heterogeneities. *Natural Hazards and Earth System Sciences*, 6(1), 89–96.

<https://doi.org/10.5194/nhess-6-89-2006>

Barthélemy, S., Bernardie, S., & Grandjean, G. (2025). Assessing rainfall threshold for

shallow landslides triggering: A case study in the Alpes Maritimes region, France.

*Natural Hazards*, 121(4), 4023–4049. <https://doi.org/10.1007/s11069-024-06941-2>

Bauer, J., Fuemmeler, S., Wooten, R., Witt, A., Gillon, K., Douglas, T., Eberhardt, E., Froese, C., Turner, K., & Lerouell, S. (2012). Landslide hazard mapping in North Carolina–Overview and improvements to the program. *Landslides and Engineered Slopes: Protecting Society through Improved Understanding. 11th International Symposium on Landslides and 2nd North American Symposium on Landslides*, 257–263.

Bogaard, T., & Greco, R. (2018). Invited perspectives: Hydrological perspectives on precipitation intensity-duration thresholds for landslide initiation: Proposing hydro-meteorological thresholds. *Natural Hazards and Earth System Sciences*, 18(1), 31–39. <https://doi.org/10.5194/nhess-18-31-2018>

Breiman, L. (2001). Random Forests. *Machine Learning*, 45(1), 5–32.  
<https://doi.org/10.1023/A:1010933404324>

Brier, G. W. (1950). VERIFICATION OF FORECASTS EXPRESSED IN TERMS OF PROBABILITY. *Monthly Weather Review*, 78(1), 1–3.  
[https://doi.org/10.1175/1520-0493\(1950\)078%253C0001:VOFEIT%253E2.o.CO;2](https://doi.org/10.1175/1520-0493(1950)078%253C0001:VOFEIT%253E2.o.CO;2)

Burrough, P., & McDonnell, R. (1998). *Principle of Geographic Information Systems*.

Chan, H.-C., Chen, P.-A., & Lee, J.-T. (2018). Rainfall-Induced Landslide Susceptibility Using a Rainfall–Runoff Model and Logistic Regression. *Water*, 10(10), 1354.  
<https://doi.org/10.3390/w10101354>

Chen, T., & Guestrin, C. (2016). XGBoost: A Scalable Tree Boosting System. *Proceedings of the 22nd ACM SIGKDD International Conference on Knowledge Discovery and Data Mining*, 785–794. <https://doi.org/10.1145/2939672.2939785>

- Crozier, M. J. (2010). Deciphering the effect of climate change on landslide activity: A review. *Geomorphology*, 124(3–4), 260–267.  
<https://doi.org/10.1016/j.geomorph.2010.04.009>
- Fan, L., Lehmann, P., Zheng, C., & Or, D. (2020). Rainfall Intensity Temporal Patterns Affect Shallow Landslide Triggering and Hazard Evolution. *Geophysical Research Letters*, 47(1), e2019GL085994. <https://doi.org/10.1029/2019GL085994>
- Froude, M. J., & Petley, D. N. (2018). Global fatal landslide occurrence from 2004 to 2016. *Natural Hazards and Earth System Sciences*, 18(8), 2161–2181.  
<https://doi.org/10.5194/nhess-18-2161-2018>
- Fuemmeler, S. J. (2008, April 10). *Landslide Hazard Mapping Methodology and Examples from North Carolina*. The Geological Society of America: Southeastern Section - 57th Annual Meeting.  
[https://gsa.confex.com/gsa/2008SE/webprogram/Paper136714.html?utm\\_source=chatgpt.com](https://gsa.confex.com/gsa/2008SE/webprogram/Paper136714.html?utm_source=chatgpt.com)
- Gariano, S. L., & Guzzetti, F. (2016). Landslides in a changing climate. *Earth-Science Reviews*, 162, 227–252. <https://doi.org/10.1016/j.earscirev.2016.08.011>
- Hatcher, R. D. (2010). The Appalachian orogen: A brief summary. In R. P. Tollo, M. J. Bartholomew, J. P. Hibbard, & P. M. Karabinos, *From Rodinia to Pangea: The Lithotectonic Record of the Appalachian Region*. Geological Society of America.  
[https://doi.org/10.1130/2010.1206\(01\)](https://doi.org/10.1130/2010.1206(01))
- Horn, B. K. P. (1981). Hill shading and the reflectance map. *Proceedings of the IEEE*, 69(1), 14–47. <https://doi.org/10.1109/PROC.1981.11918>

- Jaboyedoff, M., Michoud, C., Derron, M.-H., Voumard, Jérémie, Leibundgut, G., Sudmeier-Rieux, K., Nadim, F., & Leroi, E. (2016). *Human-Induced Landslides: Toward the analysis of anthropogenic changes of the slope environment* (pp. 217–232).  
<https://doi.org/10.1201/b21520-20>
- Kang, J., Wan, B., Gao, Z., Zhou, S., Chen, H., & Shen, H. (2024). Research on machine learning forecasting and early warning model for rainfall-induced landslides in Yunnan province. *Scientific Reports*, 14(1), 14049.  
<https://doi.org/10.1038/s41598-024-64679-0>
- Khan, S., Kirschbaum, D. B., Stanley, T. A., Amatya, P. M., & Emberson, R. A. (2022). Global Landslide Forecasting System for Hazard Assessment and Situational Awareness. *Frontiers in Earth Science*, Volume 10-2022.  
<https://doi.org/10.3389/feart.2022.878996>
- Khashchevskaya, D., Owen, L. A., Wegmann, K., Scheip, C., & Figueiredo, P. M. (2025). The characteristics and timing of multiphase major landslides along the Blue Ridge Escarpment of the southern Appalachians revealed by combined cosmogenic nuclide dating and Schmidt hammer rebound measurements. *Geomorphology*, 485, 109857. <https://doi.org/10.1016/j.geomorph.2025.109857>
- Kirschbaum, D. B., Adler, R., Hong, Y., Kumar, S., Peters-Lidard, C., & Lerner-Lam, A. (2012). Advances in landslide nowcasting: Evaluation of a global and regional modeling approach. *Environmental Earth Sciences*, 66(6), 1683–1696.  
<https://doi.org/10.1007/s12665-011-0990-3>

Kirschbaum, D., & Stanley, T. (2018). Satellite-Based Assessment of Rainfall-Triggered Landslide Hazard for Situational Awareness. *Earth's Future*, 6(3), 505–523.

<https://doi.org/10.1002/2017EF000715>

Klose, M., Damm, B., & Terhorst, B. (2015). Landslide cost modeling for transportation infrastructures: A methodological approach. *Landslides*, 12(2), 321–334.

<https://doi.org/10.1007/s10346-014-0481-1>

Klose, M., Maurischat, P., & Damm, B. (2016). Landslide impacts in Germany: A historical and socioeconomic perspective. *Landslides*, 13(1), 183–199.

<https://doi.org/10.1007/s10346-015-0643-9>

Lee, S., Oh, S., Ray, Ram. L., Lee, Y., & Choi, M. (2023). Three-dimensional hydrological thresholds to predict shallow landslides. *Terrestrial, Atmospheric and Oceanic Sciences*, 34(1), 20.

<https://doi.org/10.1007/s44195-023-00052-4>

Lin, S., Chen, S., Rasanen, R. A., Zhao, Q., Chavan, V., Tang, W., Shanmugam, N., Allan, C., Braxtan, N., & Diemer, J. (2024). Landslide Prediction Validation in Western North Carolina After Hurricane Helene. *Geotechnics*, 4(4), 1259–1281.

<https://doi.org/10.3390/geotechnics4040064>

Longley, P. A., Goodchild, M. F., Maguire, D. J., & Rhind, D. W. (2015). *Geographic Information Science and Systems*. Wiley.

[https://books.google.com/books?id=C\\_EwBgAAQBAJ](https://books.google.com/books?id=C_EwBgAAQBAJ)

Lundberg, S., & Lee, S.-I. (2017). *A Unified Approach to Interpreting Model Predictions*

(Version 2). arXiv. <https://doi.org/10.48550/ARXIV.1705.07874>

Mondini, A. C., Guzzetti, F., & Melillo, M. (2023). Deep learning forecast of rainfall-induced shallow landslides. *Nature Communications*, 14(1), 2466.

<https://doi.org/10.1038/s41467-023-38135-y>

NASA Earth Observatory. (2021, June 10). *Machine Learning Model Doubles Accuracy of Global Landslide 'Nowcasts'—NASA*.

<https://www.nasa.gov/missions/gpm/machine-learning-model-doubles-accuracy-of-global-landslide-nowcasts/>

National Hurricane Center. (2025). *Tropical Cyclone Report: Hurricane Helene (AL092024)* (p. 17).

North Carolina Department of Environmental Quality. (2024). *North Carolina Landslide Inventory Points* [Dataset]. NC OneMap.

[https://www.nconemap.gov/datasets/01965a193482438cb70332e5e524e38b\\_o/about](https://www.nconemap.gov/datasets/01965a193482438cb70332e5e524e38b_o/about)

Office of State Budget and Management. (2024). *Hurricane Helene Damage and Needs Assessment*.

[https://www.osbm.nc.gov/hurricane-helene-dna/open?utm\\_source=chatgpt.com](https://www.osbm.nc.gov/hurricane-helene-dna/open?utm_source=chatgpt.com)

Pennington, C., Dijkstra, T., Lark, M., Dashwood, C., Harrison, A., & Freeborough, K. (2014). Antecedent Precipitation as a Potential Proxy for Landslide Incidence in South West United Kingdom. In K. Sassa, P. Canuti, & Y. Yin (Eds.), *Landslide Science for a Safer Geoenvironment* (pp. 253–259). Springer International Publishing.

[https://doi.org/10.1007/978-3-319-04999-1\\_34](https://doi.org/10.1007/978-3-319-04999-1_34)

Petley, D. (2012). Global patterns of loss of life from landslides. *Geology*, 40(10), 927–930.

<https://doi.org/10.1130/G33217.1>

Petley, D. (2025, January 6). Global fatal landslides in 2024. *Eos*.

<https://eos.org/thelandslideblog/fatal-landslides-in-2024>

PRISM Climate Group. (2024). *PRISM Daily Precipitation Data (1981–present)* [Dataset].

Oregon State University. <https://prism.oregonstate.edu/>

Regorda, A., Lardeaux, J.-M., Roda, M., Marotta, A. M., & Spalla, M. I. (2020). How many subductions in the Variscan orogeny? Insights from numerical models. *Geoscience Frontiers*, 11(3), 1025–1052.

<https://doi.org/10.1016/j.gsf.2019.10.005>

Sidle, R. C., & Ochiai, H. (2006). *Landslides: Processes, Prediction, and Land Use* (Vol. 18).

American Geophysical Union. <https://doi.org/10.1029/WM018>

Sim, K. B., Lee, M. L., Rasa RemenYTE-Prescott, & Soon Yee Wong. (2022, August). *An Overview of Causes of Landslides and Their Impact on Transport Networks*. Advances in modelling to improve network resilience,

<https://op.europa.eu/en/publication-detail/-/publication/c81e8bc9-1469-11ed-8fa0-01aa75ed71a1/language-en>.

[https://www.researchgate.net/publication/369437132\\_An\\_Overview\\_of\\_Causes\\_of\\_Landslides\\_and\\_Their\\_Impact\\_on\\_Transport\\_Networks](https://www.researchgate.net/publication/369437132_An_Overview_of_Causes_of_Landslides_and_Their_Impact_on_Transport_Networks)

Stanley, T. A., Kirschbaum, D. B., Benz, G., Emberson, R. A., Amatya, P. M., Medwedeff, W., & Clark, M. K. (2021). Data-Driven Landslide Nowcasting at the Global Scale.

*Frontiers in Earth Science*, 9, 640043. <https://doi.org/10.3389/feart.2021.640043>



- Thomas, M. A., Collins, B. D., & Mirus, B. B. (2019). Assessing the Feasibility of Satellite-Based Thresholds for Hydrologically Driven Landsliding. *Water Resources Research*, 55(11), 9006–9023. <https://doi.org/10.1029/2019WR025577>
- Tiranti, D., & Rabuffetti, D. (2010). Estimation of rainfall thresholds triggering shallow landslides for an operational warning system implementation. *Landslides*, 7(4), 471–481. <https://doi.org/10.1007/s10346-010-0198-8>
- U.S. Census Bureau. (2022). *Cartographic Boundary Shapefiles – Counties* [Dataset]. <https://www.census.gov/geographies/mapping-files/time-series/geo/cartographic-boundary.html>
- U.S. Department of Agriculture, Natural Resources Conservation Service. (2024). *Soil Survey Geographic (SSURGO) Database* [Dataset]. <https://websoilsurvey.nrcs.usda.gov/app/>
- U.S. Geological Survey. (2021). *National Land Cover Database (NLCD) 2021* [Dataset]. <https://www.usgs.gov/centers/eros/science/national-land-cover-database>
- U.S. Geological Survey. (2022). *3D Elevation Program (3DEP), 1/3 arc-second DEM seamless products* [Dataset]. <https://www.sciencebase.gov/catalog/item/627f3798d34e3bef0c9a3198>
- Watterson, N. A., & Jones, J. A. (2006). Flood and debris flow interactions with roads promote the invasion of exotic plants along steep mountain streams, western Oregon. *Geomorphology*, 78(1–2), 107–123. <https://doi.org/10.1016/j.geomorph.2006.01.019>

- Wooten, R. M., Gillon, K. A., Witt, A. C., Latham, R. S., Douglas, T. J., Bauer, J. B., Fuemmeler, S. J., & Lee, L. G. (2008). Geologic, geomorphic, and meteorological aspects of debris flows triggered by Hurricanes Frances and Ivan during September 2004 in the Southern Appalachian Mountains of Macon County, North Carolina (southeastern USA). *Landslides*, 5(1), 31–44.  
<https://doi.org/10.1007/s10346-007-0109-9>
- Xiao, X., Zou, Y., Huang, J., Luo, X., Yang, L., Li, M., Yang, P., Ji, X., & Li, Y. (2024). An interpretable model for landslide susceptibility assessment based on Optuna hyperparameter optimization and Random Forest. *Geomatics, Natural Hazards and Risk*, 15(1), 2347421. <https://doi.org/10.1080/19475705.2024.2347421>
- Ye, C., Wu, H., Oguchi, T., Tang, Y., Pei, X., & Wu, Y. (2025). Physically Based and Data-Driven Models for Landslide Susceptibility Assessment: Principles, Applications, and Challenges. *Remote Sensing*, 17(13), 2280.  
<https://doi.org/10.3390/rs17132280>
- Zheng, W., Fan, W., Cao, Y., Nan, Y., & Jing, P. (2025). Landslide Hazard Assessment Under Record-Breaking Extreme Rainfall: Integration of SBAS-InSAR and Machine Learning Models. *Remote Sensing*, 17(13), 2265. <https://doi.org/10.3390/rs17132265>